HHS Public Access

Author manuscript

Nat Biomed Eng. Author manuscript; available in PMC 2019 April 25.

Published in final edited form as:

Nat Biomed Eng. 2018 December ; 2(12): 955–967. doi:10.1038/s41551-018-0280-4.

Contractile deficits in engineered cardiac microtissues as a result of MYBPC3 deficiency and mechanical overload

Zhen Ma[1,2,*,∞], **Nathaniel Huebsch**[1,2,*,†], **Sangmo Koo**[3,*,#], **Mohammad A. Mandegar**[4,5,6], **Brian Siemons**[1], **Steven Boggess**[7], **Bruce R. Conklin**[4,5,6], **Costas P. Grigoropoulos**[3], and **Kevin E. Healy**[1,2,8,§]

[1]Department of Bioengineering, University of California, Berkeley, CA

[2]California Institute for Quantitative Biosciences, Berkeley, CA

[3]Department of Mechanical Engineering, University of California, Berkeley, CA

[4]Gladstone Institute of Cardiovascular Disease, San Francisco, CA

[5]Department of Medicine, University of California, San Francisco, CA

[6]Department of Cellular and Molecular Pharmacology, University of California, San Francisco, CA

[7]Department of Chemistry, University of California, Berkeley, CA

[8]Department of Material Science and Engineering, University of California, Berkeley, CA

Abstract

The integration of in vitro cardiac tissue models, human induced pluripotent stem cells (hiPSCs) and genome-editing tools allows for the enhanced interrogation of physiological phenotypes and

§**Corresponding author:** Kevin E. Healy, kehealy@berkeley.edu.
*These authors contributed equally to this work.
∞Current affiliation: Department of Biomedical & Chemical Engineering, Syracuse Biomaterials Institute, Syracuse University, Syracuse, NY
†Current affiliation: Department of Biomedical Engineering, Washington University in St. Louis, St. Louis, Missouri
#Current affiliation: Department of Mechanical Engineering, Incheon National University, Incheon, South Korea

Data availability

The authors declare that all data supporting the findings of this study are available within the paper and its Supplementary Information. Source data for the figures are available from the corresponding author on reasonable request.

Code availability

The software for motion-tracking analysis is available at https://gladstone.org/46749d811.
The software for quantitative sarcomere analysis is available on request.

AUTHOR CONTRIBUTIONS

Z.M., S.K., N.H. and K.E.H. conceived and designed the sample fabrication and experiments. Z.M. performed biological experiments and analyzed data. N.H. performed gene expression, GCaMP6 analysis and quantitative fluorescent microscopy studies for identifying the molecular basis. S.K. fabricated the filamentous matrices, performed the COMSOL analysis, and wrote the MATLAB script for force measurement. N.H. developed the software for quantitative sarcomere analysis, and the motion-tracking software for contractility analysis. M.A.M. developed the MYBPC3 hiPSC lines using TALEN-mediated genome editing method. B.S. helped with hiPSC culturing, hiPSC-CMs differentiation and characterization. Z.M., N.H., S.K., and K.E.H. wrote the manuscript with discussions and improvements from all authors. K.E.H., B.R.C. and C.P.G. funded the study, and C.P.G., B.R.C. and K.E.H. supervised the project development and management.

COMPETING INTERESTS

The other authors declare no competing financial interests.

the recapitulation of disease pathologies. Here, in a cardiac tissue model consisting of filamentous 3D matrices populated with cardiomyocytes (CMs) derived from healthy wild-type hiPSCs (WT hiPSC-CMs) or from isogenic hiPSCs deficient in the sarcomere protein cardiac myosin binding protein C (MYBPC3$^{-/-}$ hiPSC-CMs), we show that the WT microtissues adapted to the mechanical environment with increased contraction force commensurate to matrix stiffness, whereas the MYBPC3$^{-/-}$ microtissues exhibited impaired force-development kinetics regardless of matrix stiffness and deficient contraction force only when grown on matrices with high fiber stiffness. Under mechanical overload, the MYBPC3$^{-/-}$ microtissues had a higher degree of calcium transient abnormalities, and exhibited an accelerated decay of calcium dynamics as well as calcium desensitization, which accelerated when contracting against stiffer fibers. Our findings suggest that MYBPC3 deficiency and the presence of environmental stresses synergistically lead to contractile deficits in the cardiac tissues.

Myosin binding protein-C cardiac isoform (MYBPC3) is a thick filament accessory protein of the striated muscle sarcomere A-band, and mutations in MYBPC3 are implicated in both Hypertrophic Cardiomyopathy (HCM) and Dilated Cardiomyopathy (DCM)[1]. The molecular mechanisms by which MYBPC3 mutations lead to the contractile deficits for DCM phenotypes remain elusive, while increasing reports from mouse models indicated that stress played a role in the initiation and progression of the physiopathology process associated with MYBPC3 mutations[2]. Currently, hiPSC technology has provided previously unanticipated possibilities to model human heart diseases in cell culture, but these models have tended to simplify the diseases as monogenic, hereditary forms of diseases, which neglects the diversity in disease phenotypes resulting from genetic-environmental interactions. Mechanical cues such as afterload, play a particularly important role in the normal function of the heart and the pathogenesis of diseases like cardiomyopathy. Incorporating environmental stresses such as mechanical cues into engineered hiPSC-based tissue models would provide the opportunity to model disease phenotypes with high precision.

3D engineered cardiac tissue models that mimic native tissue structures have been developed using a variety of methodologies and materials, which share a common process of hiPSC-CMs encapsulation into external hydrogels[3,4]. To promote hiPSC-CMs alignment and formation of physiologically relevant tissue structures, the 3D cardiac tissues are anchored between two flexible cantilevers, which also served as a force sensor[5–7]. However, this measurement is compromised by the complex mechanical and biochemical contribution of extracellular matrix (ECM) hydrogels such as collagen, which alter tissue formation, mechanical properties[8] and cellular contractile forces[8]. Therefore, self-assembled cardiac tissues relying on endogenous secretion of a cardiac specific extracellular matrices (cECM) are being explored for more consistent tissue self-assembly and remodeling[9].

The biophysical microenvironment plays a critical role in cardiac pathophysiology. For example, the afterload against which the heart contracts directly relates to the mechanical stretch on CMs and plays an important role in the pathogenesis of DCM[10]. Contraction force, a key component of cardiac function, is continuously regulated by the surrounding environment[11]. The contraction force of hiPSC-CMs has been deemed as one of the essential

parameters for the evaluation of normal mature cardiac function, response to pharmacological interventions, and indication of disease phenotypes[12–14]. The force sensors used in the cardiac tissue models not only reported the contraction forces generated by hiPSC-CMs, but also naturally becomes the external mechanical load that regulates the cardiac tissue remodeling and function. In traction force microscopy, variation of substrate stiffness altered the myofibril organization of 2D micropatterned hiPSC-CMs, demonstrating substrata with optimal stiffness improved the contractile activity of hiPSC-CMs[15]. In 3D cardiac tissue models, flexible cantilevers used to anchor cardiac tissues also presented a rigid external structure to mimic *in vitro* cardiac tissue afterload[16]. Increase of the mechanical load to hiPSC-CMs from patient-specific and genome-engineered hiPSCs facilitated better modeling of DCM associated with TTN gene mutations[17]. In contrast, optimal mechanical load was critical for the 3D maintenance and maturation of hiPSC-CMs with highly organized sarcomeres, as well as increased adherens and gap junction formation[18].

To address the hypothesis that tissue mechanical resistance to contraction can regulate CM sensitivity to the loss of MYBPC3, in the absence of complex interactions between cells and natural ECM derived gels, we created a cardiac tissue model that employed highly ordered 3D fibers. The structure and mechanical properties of these fibers promoted cardiac tissue self-assembly and dynamic remodeling. Using two-photon polymerization (TPP), we created different filamentous matrices by fabricating precisely defined, ultra-high aspect ratio synthetic parallel fibers with different fiber diameters (*i.e.*, 5 μm and 10 μm). Although these fibers have constant elastic modulus, the thicker fibers have a higher mechanical resistance to cellular contraction than thinner fibers. We populated WT hiPSC-CMs, or isogenic MYBPC3$^{-/-}$ hiPSC-CMs that completely lack expression of the sarcomere protein MYBPC3. WT cardiac microtissues adapted their contraction velocity and contraction force to the alternations of mechanical load. In contrast, MYBPC3$^{-/-}$ cardiac microtissues exhibited impaired force relaxation kinetics, but only exhibited defects in total systolic contractile force, compared to WT microtissues, when challenged with stiffer fibers. These results suggest that the cardiac tissue's mechanical microenvironment facilitated the modeling of contractile deficits associated with the absence of MYBPC3 protein. Incorporation of appropriate mechanical resistance to cardiac contractility will likely be an important aspect of future efforts to model human heart disease *in vitro*.

RESULTS

Matrix fabrication and cardiac microtissue self-assembly and remodeling

Filamentous matrices were fabricated using TPP that produced scaffolds with highly defined micro and nano-scale features (Figure S1a, Movie S1)[19–21]. Based on previous studies, we concluded that the filamentous matrices, consisting of parallel fibers with 500 μm fiber length in Y-axis direction, 50 μm fiber spacing in X-axis direction, and 30 μm layer spacing in Z-axis, could robustly generate 3D condensed cardiac microtissues[22] (Figure S1b). In this study, we fabricated multiple matrices within one pair of glass coverslips by separating cohorts of fiber matrices with 2 mm spacing in X-axis (Figure S1b). This design not only increased the throughput, but also made the fiber deflection easier to measure for contraction

force calculations. Scanning electron microscopy confirmed a matrix with parallel fibers, and the ability to control fiber diameter (*e.g.*, 5 μm and 10 μm) (Figure S1c).

We seeded hiPSC-CMs onto filamentous matrices without any additional cell-encapsulating ECM gel. Generation of 3D cardiac microtissues required a relatively purified hiPSC-CM population and consistent cell handling procedures (Figure S2a). Purification procedures[23,24] can routinely produce highly purified CM populations (cTnT+ cells > 95%). However, 3D engineered cardiac microtissues require a stromal cell or fibroblast population to enhance the mechanical integrity and connectivity of tissues[9,25,26]. Instead of six days of treatment with lactate purification media, we treated our cells for only four days, which resulted in a mixed hiPSC-CMs population (TNNT2+ cells ~ 80%, Figure S2b–c).

The hiPSC-CMs seeded on the filamentous matrices self-assembled into 3D cardiac microtissues (Z-axis thickness ~ 60 μm, Figure S3a,b) and maintained a stable beat rate after 5-day of culturing. The cardiac microtissues continuously and progressively remodeled in response to the passive mechanical load of the fibers and active tissue contraction. The beat rate, contraction velocity, contraction force, and width of the individual cardiac microtissues were measured every 5 days to track the tissue remodeling associated with the change of functional readouts. Since the individual fibers were fixed onto the glass coverslips at both ends, the contracting cardiac microtissues were only able to deform the fibers in the X-direction, but not in Y-direction (Movie S2). This mechanical constraint resulted in the anisotropic contraction with higher contraction along the X-axis compared to the Y-axis, as defined by contraction heatmaps (Figure 1a). We calculated the ratio of contraction velocity in the X and Y directions, and found a significant increase in the ratio from Day 5 to Day 20 (Figure 1b). We also observed that the microtissues condensed in the direction of the Y-axis, but maintained the integrity along the X-axis, resulting in a significant decrease in the tissue cross-section areas (Z-Y direction) from Day 5 to Day 10 – 20 (Figure 1c). This data suggested that the change in tissue shape occurred simultaneously with the orientation of the contraction directions, thus anisotropic contraction and anisotropic tissue shape reinforced each other during the tissue remodeling process.

Mechanical load affected cardiac microtissue contractile functions

To test the hypothesis that mechanical overloading influences cardiac tissue functions, we created matrices with different fiber diameter. By changing fiber diameter, we could change the fiber bending stiffness to modulate the mechanical load to the cardiac microtissues assembled around the fibers. Based on atomic force microscopy (AFM) calibration of individual fibers, we calculated the elastic modulus of the material as 183.9 ± 11.7 MPa, which refers to the linear ratio of force load and deformation of the fiber. Although the elastic modulus is the same for both fibers, the fiber bending stiffness against which cells must contract is proportional to the square of fiber diameter, thus 5 μm fibers are much easier to be bend compared to 10 μm fibers. We did not observe a significant difference in the beat rate of the cardiac microtissues between 5 μm matrices and 10 μm matrices, but the beat rate slightly increased from Day 5 – 10 to Day 15 – 20 (Figure 1d). Likely because 5 μm fibers are easier to be bend, we found higher maximal contraction velocity for cardiac microtissues assembled on the 5 μm matrices compared to 10 μm matrices (Figure 1e). This

data suggested that modulating the mechanical load of tissue microenvironment via changing the fiber bending stiffness altered the contractile functions of cardiac microtissues.

We used the deflection of individual fibers to calculate the force of contraction. By assuming all the forces throughout the tissue cross-section were evenly distributed and parallel (Figure S4a), we calculated the point force exerted on individual fiber based on the fiber deflection and force position (where the maximal deflection locates) measured in a series of recorded images (Figure S4b). Using this point force, we could also calculate the total force generated by the cardiac microtissues. Through theoretical calculations, we found that the force measured by 10 μm fiber was approximately 10-fold higher than the force measured by 5 μm fiber with the same fiber deflection and force position (Figure S4d,e). Therefore, artificially applying the forces at the center region of the fiber with 1 μN to a 5 μm fiber and 10 μN to a 10 μm fiber, we could determine the stress generated on the fibers through COMSOL numerical simulation. High stress occurred at the center region of the fiber, where the force was applied, and also occurred at two ends of the fiber, where the fiber was fixed at both sides of the glass coverslips (Figure S4c, Movie S3).

Cardiac preload is defined as end-diastolic myocardial wall tension. In this study, we refer to preload as the passive tension exerted by the fibers at two edges of the matrix to the diastolic cardiac microtissue at the resting state. The load opposing shortening of the ventricular muscles is termed cardiac afterload. Here, the cardiac tissue afterload is defined as the fiber tension against the systolic cardiac microtissue at the maximal contraction (Figure 2a). The afterload considerably increases when the cardiac microtissues contract against the stiffer fibers. Based on the fiber deflections – force relationship discussed above, we calculated the static forces (diastole) and contraction forces (systole) for the cardiac microtissues assembled on both 5 μm and 10 μm matrices, and found that cardiac microtissues produced higher forces when grown on the matrices with stiffer. We found that the static forces increased significantly from Day 5 to Day 20 for the cardiac microtissues assembled on both 5 μm and 10 μm matrices (Figure 2b,c), whereas the contraction forces increased significantly only when the microtissues grew on the 10 μm matrices, not on the 5 μm matrices (Figure 2d,e). Self-assembled WT hiPSC-CMs on the 10 μm filamentous matrices adapted to the high stiffness and increased the contraction force through mechanical overloading.

Isogenic MYBPC3$^{-/-}$ cardiac microtissues exhibit force deficits without structural disarray

To test the hypothesis that mechanical resistance synergizes with genetics to cause contraction deficits, we harnessed TALEN-assisted gene-editing to create an isogenic human homozygous MYBPC3 null cardiac microtissue model. MYBPC3 is a thick filament associated protein, which is thought to play a principally structural role for stabilization of the sarcomere sliding during contraction[27,28] (Figure S5a). Fluorescent images of WT hiPSC-CMs showed the MYBPC3 protein aligned with ATCN2 protein, indicating the structural relationship of A bands and Z discs (Figure S5b). Furthermore, this protein binds to thin and thick filaments, thereby regulating the probability of cross-bridge interactions, which in turn controls the rate of force development and relaxation in cardiac muscles[29].

To test the hypothesis that environmental conditions could modulate the contraction deficits caused by loss-of-function mutations, we focused this initial study on a severe loss-of-function caused by complete, homozygous knockout of MYBPC3. The isogenic homozygous MYBPC3$^{-/-}$ hiPSC cell line was developed using TALEN-based genome editing (Figure S5c). hiPSC-CMs derived from MYBPC3$^{-/-}$ hiPSC parent cells showed a complete loss of MYBPC3 mRNA and protein (Figure S5e,f). MYBPC3$^{-/-}$ hiPSC-CMs formed the 3D anisotropic cardiac microtissues on both 5μm and 10μm filamentous matrices (Movie S4), so we could determine how mechanical overload affected the contractile behaviors in MYBPC3$^{-/-}$ cardiac microtissues. There was no significant difference in the static forces between WT and MYBPC3$^{-/-}$ cardiac microtissues on both 5 μm and 10 μm matrices (Figure 3a,b), which suggested the absence of MYBPC3 had no effect on cardiac preload. Furthermore, we did not observe a difference in the contraction forces between MYBPC3$^{-/-}$ and WT cardiac microtissues on 5μm fibers. However, we observed a marked inhibition in contractile force development in MYBPC3$^{-/-}$ cardiac microtissues, compared to WT, on 10μm fiber matrices (Figure 3c,d). We also found that the MYBPC3$^{-/-}$ cardiac microtissues showed higher contraction velocity compared to WT, and this velocity difference between WT and MYBPC3$^{-/-}$ cardiac microtissues was exaggerated on 10 μm matrices (Figure 3e,f). Independent of either tissue type, the magnitude of force was greater on 10 μm matrices and the contraction velocities were significantly higher on 5 μm matrices. These results suggested that modulating the mechanical load against which engineered cardiac tissue contracted facilitated the manifestations of contractile deficits due to absence of MYBPC3 protein. To rule out any effects of contraction abnormalities on these results, we only assessed the force of systolic contraction in microtissues that had regular beating behaviors, defined *SD/mean* of beating relaxation decay time less than 0.1.

Since we found substantial reduction of contraction forces from MYBPC3$^{-/-}$ cardiac microtissues on 10 μm matrices, we subsequently evaluated the structural characteristics between WT and MYBPC3$^{-/-}$ cardiac microtissues on 5 μm and 10 μm matrices at Day 20 (Figure 4a,c). Surprisingly, we found no significant differences on tissue cross-section areas (Figure 4b), sarcomere organization (Figure 4d,e) and connexin 43 (Cx43) expression (Figure S6) from either of the two genotypes or fiber matrix types. These results suggested that absence of MYBPC3 protein did not induce gross tissue shape remodeling or sarcomere disarray at the *in vitro* tissue level within 20-day culture, but did play an important role in force development responding to the external mechanical overload.

Isogenic MYBPC3$^{-/-}$ cardiac microtissues exhibit abnormalities in force and calcium dynamics

As structural deficiencies were not sufficient to explain the marked force deficits in MYBPC3$^{-/-}$ cardiac microtissues on stiff fiber matrices, next investigated contractile force kinetics. Since MYBPC3 protein is thought to regulate the force development during cardiac contraction[30], we plotted the force kinetics curves for WT and MYBPC3$^{-/-}$ cardiac microtissues on 5 μm and 10 μm matrices at Day 20. By multiplying the force and velocity, we also plotted the power kinetics curves, and measured the area under the curve as the total energy consumed by the cardiac microtissues to complete one contraction. On both 5 μm and 10 μm matrices, MYBPC3$^{-/-}$ cardiac microtissues developed the maximal contraction

forces faster than WT microtissues (Figure 5a,c). Since the force magnitude was similar between WT and MYBPC3$^{-/-}$ cardiac microtissues on the 5 μm matrices, higher contraction velocity led to higher power output and more energy consumption (the area of power kinetics curve) of the MYBPC3$^{-/-}$ cardiac microtissues (Figure 5b). On the other hand, MYPBC3$^{-/-}$ cardiac microtissues on the 10 μm matrices developed significantly lower contraction forces, less power output, but similar energy consumption compared to the WT microtissues (Figure 5c,d). The same energy consumption, but low force production from MYBPC3$^{-/-}$ cardiac microtissues indicated that absence of MYBPC3 protein impaired the cardiac microtissues to contract in an energy-efficient manner. To further analyze the force kinetics, we measured the upstroke time to peak force (τ_{max}), early decay time of 50% peak force (τ_{50}) and late decay time of 75% peak force (τ_{75}). We found no significant difference of the cardiac microtissues between 5 μm and 10 μm fiber matrices, but MYBPC3$^{-/-}$ cardiac microtissues were statistically faster to reach to the peak force (τ_{max}, Figure 5e). Compared to the WT microtissues, MYBPC3$^{-/-}$ microtissues exhibited no significant difference on early decay time (τ_{50}, Figure 5f), but a slower late decay time (τ_{75}, Figure 5g). This delayed force relaxation is consistent with an HCM-like phenotype[1].

Previous studies have noted that hiPSC-CMs derived from patients with familial cardiomyopathy are more prone to electrophysiological abnormalities such as Early After Depolarizations (EADs)[31]. To determine how the abnormalities on the calcium handling occurred on MYBPC3$^{-/-}$ cardiac microtissues under mechanical overload, we generated hiPSC harboring the genetically-encoded Ca^{2+} reporter, GCaMP6f, which was inserted into the AAVS1 locus on both WT and MYBPC3$^{-/-}$ hiPSC lines (Figure S5d), allowing direct measurements of calcium dynamics. The fluorescent fluctuation of GCaMP6f signal from the GCaMP6f cardiac microtissue assembled on the filamentous matrices indicated the Ca^{2+} dynamics of the cell, (Figure 6a and Movie S5), caused by the combination of L- type calcium channels and calcium-induced calcium release from the sarcoplasmic reticulum, downstream of the action potential[32].

We generated GCaMP6f-WT and GCaMP6f-MYBPC3$^{-/-}$ cardiac microtissues on both 5 μm and 10 μm matrices, and recorded the calcium transient via the GCaMP6f reporter (Figure 6b). We first analyzed calcium dynamics in the microtissues that did not exhibit gross calcium transient abnormalities (this was defined by measuring the decay time, τ_{75}, of the calcium transient, and selecting tissues with SD/mean $\tau_{75} < 0.1$). Within this set of tissues, we found that there was no effect of MYBPC3 deficiency on the overall intensity of GCaMP, suggesting that the overall amount of Ca^{2+} entering cells remained the same. However, we did observe increased GCaMP maximum, corresponding to greater calcium intake, when both WT and MYBPC3 deficient tissues were challenged to contract against stiffer fibers (Figure 6c). By analyzing calcium transient decay dynamics, we observed no significant difference on early decay time (τ_{50}, Figure 6d), but did find that MYBPC3$^{-/-}$ cardiac microtissues on both 5μm and 10μm fiber matrices exhibited faster late decay times (τ_{75}) of calcium transient compared to WT microtissues (Figure 6e).

Although EADs were rare events in all microtissues (Figure 6f), we did observe a significantly increased probability of EAD events in MYBPC3$^{-/-}$ microtissues contracting against stiff fibers (Figure 6g,h). We also analyzed the calcium sensitivity of GCaMP6f-WT

and GCaMP6f-MYBPC3$^{-/-}$ cardiac microtissues on both 5 μm and 10 μm matrices, and found the trend of calcium desensitization of MYBPC3$^{-/-}$ microtissues comparing to WT microtissues (Figure 6i). More importantly, the cardiac microtissues appeared to become further desensitized to extracellular calcium when contracting against the stiffer matrices. The mismatch between faster decay of calcium transient and slower decay of contraction force indicated the importance of MYBPC3 protein for regulating the cardiac contractility through excitation-contraction coupling. This is consistent with data obtained in cell-free, reconstituted protein assays that implicate MYBPC3 protein as a potential "molecular brake" controlling the rate of force development and relaxation in heart muscle[30].

To begin to understand the mechanisms through which stiffer matrices affected pathology of MYBPC3$^{-/-}$ hiPSC-CMs, we profiled gene expression (102 genes) for the WT and MYBPC3$^{-/-}$ cardiac microtissues on 10 μm matrices (Figure 7a). Although we found no significant difference in either sarcomere structural deficit (MYH6, MYH7) or calcium handling malfunction (CALM1, CALM3), which have been typically related to HCM, we identified four genes (EP300, CREBBP, HDAC1 and GATA4) that were significantly up-regulated in the MYBPC3$^{-/-}$ microtissues (Figure 7b). We also found the expression of human brain natriuretic peptide (hBNP) between WT and MYBPC3$^{-/-}$ cardiac microtissues only became significantly different when the cardiac microtissues grew on 10 μm matrices, suggesting that the observed loss of contraction force is concurrent with molecular indicators of disease progression in the MYBPC3$^{-/-}$ microtissues (Figure 7c). Via confocal microscopy and quantitative fluorescent measurement, we determined the EP300 expression significantly increased on the cardiac microtissues grown on the 10 μm matrices compared to the ones on 5 μm matrices (Figure 7d). Furthermore, we found that EP300 expression on MYBPC3$^{-/-}$ cardiac microtissues was significant higher than WT microtissues on both 5 μm matrices and 10 μm matrices, suggesting that EP300 plays a key role in the synergy between genetic deficiency and mechanical overload in inducing contractile deficits (Figure 7e).

DISCUSSION

In this work, we combined hiPSC technology, genome editing tools, and advanced material processing to create a next-generation hiPSC-based cardiac tissue model, which recapitulated the synergism of genetic deficiencies and environmental stresses required to induce the life-threatening cardiomyopathies. We innovated the conventional TPP technique to enable fabrication of high aspect ratio (100:1) fibers with reasonable throughput, which ensured the structural support and force sensing function used in our cardiac tissue model[33]. Such aspect ratios are impossible to achieve with standard microfabrication technology. Furthermore, unlike other methods to create filamentous matrices like electrospinning, self-assembly, 3D micropatterning of hydrogels, our TPP technique have unprecedented control over a wide range of matrix features deemed important in allowing immediate cell infiltration for 3D tissue formation and regulating tissue mechanical functions[22]. Not only harnessing the mechanical load of the fiber matrix as the environmental stress to the hiPSC-CMs, we also used the genome-editing to engineer isogenic diseased hiPSC lines to precisely control the genetic background[34,35], in order to understand the pathogenesis from a specific gene mutation and its interaction with environmental stress.

Previous studies from MYBPC3 knockout mice exhibited impaired contractile properties with overall reduction in diastolic and systolic functions observed at the whole heart level[36,37]. Consistent with our hiPSC model, myofilament Ca^{2+} sensitivity of tension was also reduced in MYBPC3$^{-/-}$ mice with a right-shifted normalized Ca^{2+} tension curve relative to the WT mice. Our findings that MYBPC3$^{-/-}$ cardiac microtissues were viable and display well-developed sarcomeres, conflicting with previous hypothesis that MYBPC3 protein plays essential structural roles for sarcomere assembly and stability. However, our study was consistent with the MYBPC3$^{-/-}$ mouse model, in which the well-organized sarcomere striation patterns were observed in nearly all sections of heart tissues[36]. Our results, together with mouse models, indicated that MYBPC3 protein is not an absolute requirement for the assembly and maintenance of organized sarcomeres and myofibrils, but serves a complimentary role in modulating cardiac contractile functions.

To examine the regulatory effects of MYBPC3 protein on cardiac contractile function, multiple heterozygous and homozygous mouse models have been established with confounding results. One *in vitro* homozygous MYBPC3$^{-/-}$ mouse tissue model demonstrated characteristic acceleration of contraction kinetics, a hyper-contractile HCM-like disease phenotype[38], while another homozygous tissue model demonstrated DCM-like reduced contractions[39], indicating the complexity of genotype-phenotype correlation provoked by the MYBPC3 mutations. Recently, a tamoxifen-inducible MYBPC3$^{-/-}$ mouse model only demonstrated impaired diastolic function, but very mild systolic dysfunction under normal conditions[40]. However, if pressure overload was induced by transverse aortic constriction (TAC), these mice developed left ventricular dilation and reduced contractile functions. These results suggest that mechanical stress in the form of increased afterload may be required to observe phenotypes associated with MYBPC3 loss-of-function mutations. This is consistent with the observation that systemic resistance is a major risk factor for heart failure in the setting of cardiomyopathy[10]. These indications also lean towards the clinical findings that a subset of patients with HCM associated with heterozygous MYBPC3 truncated mutations could later develop left ventricular dilation and systolic dysfunction similar to DCM, otherwise known as “burnt out” phase HCM or end-stage HCM. However, these murine-based *in vivo* models make it very difficult to specifically isolate the biomechanical etiology underlying the disease onset and process, as TAC or other maneuvers that increase cardiac afterload also affect global signaling through inflammation and other processes[41]. In contrast, our hiPSC-based *in vitro* model eliminates the complex changes in soluble milieu related to the maneuvers used in animal models for cardiac overload, and also allows the disease process to be modeled in genetically defined human cells.

Currently, hiPSC-based MYBPC3-related disease models have only been established at single cell or 2D monolayer levels. A previous report on patient-derived hiPSC-CMs carrying a heterozygous MYBPC3 mutation (c.2373dupG) micropatterned at single-cell level showed systolic dysfunction with lower contractile force generation compared to the healthy controls[42]. Consistent with the hypothesis that MYBPC3$^{-/-}$ genotypes reduce contractile force, a recent study using an allelic series of isogenic MYBPC3$^{-/-}$ hiPSC-CMs indicated a decrease in contractile force of single hiPSC-CMs as MYBPC3 dose was reduced[43]. In light of these studies, we decided to solely focus on the MYBPC3$^{-/-}$ hiPSC-

CMs to develop an *in vitro* disease model, so that we could study how such contractile deficits due to absence of MYBPC3 protein would be altered by external mechanical overload and associated gene expression. Importantly, despite the extreme severity of homozygous loss-of-function of MYBPC3, we only observed pathological phenotypes when hiPSC-CMs were challenged to contract against overload. This suggests physical properties of the tissue microenvironment could be used as environmental stress to induce and deteriorate the contractile deficits resulted from the genetic deficiency.

In vitro modeling external mechanical load to cardiac tissues has been developed either by passive stretch of cardiac tissues mimicking the increase of preload[44,45], or stiffening the flexible cantilevers to cardiac tissues mimicking the increase of afterload[16,17,46]. It has been suggested that *in vitro* systems of engineered cardiac tissues could unmask subtle abnormalities due to genetic deficiencies that were concealed by the compensatory mechanisms in intact animals[47]. Our model facilitated 3D tissue-like arrangement of hiPSC-CMs, mimicked the increase of afterload, and assessed the effects of mechanical overload on cardiac functions. WT cardiac microtissues exhibited enhanced contractile functions in response to the increase of afterload. Furthermore, we assessed the contractile deficits of human MYBPC3$^{-/-}$ cardiac microtissues under low and high mechanical load, and found MYBPC3$^{-/-}$ microtissues only exhibited reduced systolic contraction force on the matrices with stiffer fibers. This data demonstrated that absence of MYBPC3 protein impaired physiological adaptation to the mechanical overload, induced contractile deficits, and activated pathological signaling.

Previous study on patient-derived hiPSC line harboring MYBPC3 mutation indicated myofibril disarray at single-cell level[48]. Although we observed clear functional deficits in the contractile behaviors of MYBPC3$^{-/-}$ cardiac microtissues, these did not directly correlate to marked changes in sarcomere structure, indicating that sarcomere disarray may be a consequence, rather than a cause of contractile dysfunction during the development of MYBPC mutation-related cardiomyopathies. This highlights the need for technologies, such as genetically-encoded sarcomere reporters[25], which allow researchers to *in vitro* observe the timing of consecutive sequence for different hallmarks of cardiomyopathy from contractile deficits to structural disarray, or vice versa. Potentially, the combination of biomechanical cues with chemical-induced stress or prolonged culture would lead to structural deficiencies.

To begin understanding molecular mechanisms underlying how environment alters genotype-phenotype relationships, we performed proof-of-concept gene array studies and identified EP300-CBP-GATA4 as a cascade involved in overload-induced contractile deficits on MYBPC3$^{-/-}$ cardiac microtissues. It has been previously reported that downregulation of C/EBPβ in the heart was associated with overload-induced physiological hypertrophy[49]. The deactivation of C/EBPβ pathway was associated with up-regulation of CITED4, the EP300-CBP interacting transactivator, which promoted the proliferation of CMs. In our study, we suggested that up-regulation of EP300-CBP was also associated with overload-induced contractile deficits, which was consistent with a previous study in which EP300 overexpression led to hypertrophy of cardiomyocytes and the heart *in vivo*[50]. Pathological stress, such as pressure overload, alters cardiac gene expression and promotes the activation

of gene predominantly expressed in the fetal heart. From the MYBPC3$^{-/-}$ cardiac microtissues on 10 μm matrices, we only found significant increase of GATA4 expression, although expression of MEF2C and TBX5 also showed an increasing trend, though not statistically significant ($p < 0.2$). In previous studies, heart EP300 ChIP-sequencing reads were strongly enriched on GATA4 peaks[51,52], suggesting that GATA4 directly interacted with EP300-CBP for synergistic gene activation of ANP, BNP and MYH7 promoters during myocardial hypertrophy[53,54]. In contrast to indirect means of inducing mechanical stress, such as chronic catecholamine exposure, direct manipulation of the biophysical properties of the *in vitro* cardiac microenvironment does not introduce additional signaling pathways (*e.g.* GPCR signaling) that complicate mechanistic studies.

MYBPC3 accounts for a significant proportion of familial cardiomyopathies, and is associated with both HCM and DCM. However, the molecular mechanisms linking MYBPC3 mutations to the pathogenesis of cardiomyopathy remain elusive. Our study emphasized the role of MYBPC3 protein in regulating cardiac contractile functions by using a homozygous MYBPC3 knockout isogenic hiPSC line, and demonstrated pronounced DCM-like contractile phenotypes (impaired systolic contraction force, faster decay of calcium dynamics, and calcium desensitization) on the MYBPC3$^{-/-}$ cardiac microtissues contracting against stiffer fibers. In future studies, our findings relating the importance of overload in modeling cardiomyopathy phenotypes could be leveraged to study the effects of more subtlety, heterozygous missense or truncated mutations typically found in patients. Importantly, the results obtained from this study with isogenic lines can be used as “training sets” to calibrate our system and provide “standards” for the subsequent studies on more diverse genetic backgrounds and greater variety of phenotypes.

METHODS

An expanded Methods section is included in the Supplementary Information, with more details on cell handling, motion tracking analysis, finite element modeling, immunostaining and microscopy, RT-qPCR. hBNP ELISA, flow cytometry, quantitative sarcomere analysis and statistical methods.

Fabrication of filamentous matrices

The filamentous matrices were fabricated by TPP using the photo-curable organic-inorganic hybrid polymer OrmoClear® (Micro resist technology). Briefly, OrmoClear® resin was first spin-coated, pre-baked and UV cured on the glass coverslips. Two glass coverslips with cured OrmoClear® thin layers were assembled as one set with 500 μm-thick spacers and filled with uncured OrmoClear®. Individual fibers were fabricated by single laser beam radiation of the uncured OrmoClear® through a high repetition rate femtosecond laser (pulse duration: ~ 400 femtosecond, repetition frequency: 1 MHz, wavelength: 1045 nm, FCPA μJewel D-400, IMRA America Inc.). The laser beam was frequency-doubled (wavelength: 522 nm) by Lithium triborate (LBO) second harmonic nonlinear crystal (Newlight photonics) and focused at the interface between glass coverslip and OrmoClear® with 5× objective (N.A. = 0.14) (M Plan Apo, Mitutoyo). Fiber diameter was determined by the laser power and exposure duration, which was controlled through a mechanical shutter (Thorlabs).

5 μm fibers were fabricated by 3.7 mW power laser radiation for 0.9 seconds, whereas 10 μm fibers were fabricated by 5.2 mW for 2 seconds. Fiber spacing was controllable by a 3D axis motorized stage with high precision of positioning (Aerotech, ANT95-XY-MP for X–Y axis and ANT95-50-L-Z-RH for Z axis). To fabricate several matrices within one set, we blocked the laser radiation during the movement from the end point of the previous matrix to the starting position of next matrix. After fiber fabrication, samples were hard-baked for 10 minutes, developed for 30 minutes with a mixture of 2-Isopropyl alcohol and 4-Methyl-2-pentanone (1:1, Sigma Aldrich), rinsed with 2-Isopropyl alcohol and DI water 3 times, and dipped in 70% ethanol for sterilization.

Generation of 3D cardiac microtissues

Three sets of glass devices were placed into one well of a 6-well plate, rinsed with Dulbecco's phosphate buffered saline (DPBS, Gibco) three times, and diluted Matrigel was adsorbed for at least 1 hour. Diluted Matrigel was rinsed off before cell seeding, leaving a thin coating on the individual fibers, instead of Matrigel gel. Cryopreserved hiPSC-CMs were thawed into EB20 media and plated onto Matrigel-coated 6-well plate with RPMI/B27+C media supplemented with 10 μM Y-27632. After 4 days recovery in RPMI/B27+C media, the cells were singularized by 0.25% trypsin, quenched with EB20 media, and seeded into filamentous matrices without ECM proteins or additional Matrigel at a density of 3 million/mL RPMI/B27+C media supplemented with 10 μM Y-27632. After four hours, another 4 mL RPMI/B27+C media supplemented with 10 μM Y-27632 was added into each well to cover the whole set of filamentous matrices. The media was switched to RPMI/B27+C media the next day and changed every 2 days. Videos of cardiac microtissue beating were recorded every 5 days for motion tracking analysis and force measurement.

Fiber characterization

The elastic modulus of the fiber (E_f) was measured by atomic force microscopy (AFM, XE-100, Park Systems) with tip-less AFM cantilevers (TL-CONT-SPL and TL-FM-SPL, Nanosensors). Fiber shape was assumed to be a cylinder with a circular cross-section. Hence, the Young's modulus of the fiber was calculated via equation (1).

$$E_f = \frac{64Kd_cL^3}{3\pi D^4(d_f - d_c)} \quad (1)$$

with length (L) and diameter (D) of the fiber, deflection of the AFM cantilever (d_c) and relative deflection of the fiber (d_f). The spring constants (K) of tip-less AFM cantilevers were measured using the thermal tuning method[55] and calculated to be 0.0636 N/m using AFM software (XEI, Park system). Finally, Young's modulus of the fibers with both 5 μm and 10 μm diameters was calculated to be 183.9 ± 11.7 MPa.

Force measurement

To calculate the contraction forces of the whole cardiac microtissue, we made three assumptions: (1) the forces were evenly distributed across the tissue cross-section (tissue

width multiplying tissue thickness W (y-axis)·H (z-axis)); (2) all the force vectors were parallel each other and perpendicular to the fiber axis; and, (3) the fiber had a circular cross-section. Based on those assumptions, we calculated the total force (F) generated by the cardiac microtissue by integrating the distributed force (f) across entire tissue cross-section. To calculate the generated force of whole cardiac tissue, the individual fiber point force (F') was calculate based on the beam deflection theory at the position with maximal fiber deflection. Using the series of single-frame image recorded for cardiac tissue beating, we measured the fiber deflection (δ) at specific positions (a) between two consecutive images, so that we could calculate the point force (F') applied to the fibers based on equation (2) with Young's modulus (E_f), length (L) and diameter (D) of the fiber.

$$F' = \frac{3\pi E_f D^4 (2a + L)^2}{128 a^3 (L - a)^2} \quad (2)$$

The distributed force (f) was calculated by dividing the individual fiber point force (F') by the half-cylinder surface area of the applied force to the fiber. Finally, integrating the distributed force across entire tissue cross-section, we calculated the total force (F) generated by the cardiac microtissues. The static force was calculated based on the preload fiber defection that was measured with the cardiac microtissue in the resting diastolic state, whereas the contraction force was calculated based on the afterload fiber defection that was measured with cardiac microtissue at maximal contraction, systolic state. All the contractile function analysis was performed only on the microtissues with regular contraction kinetics (normalized errors in τ_{75} less than 0.1).

Calcium transient dynamics analysis

For calcium imaging, GCaMP6f hiPSC-CMs were differentiated, purified, cryopreserved, seeded, and formed the microtissues on the filamentous matrices for continuous calcium imaging at Day 20. The calcium flux images were recorded at 30 frames per second for 10 seconds using a Nikon Eclipse TS100F microscope with temperature-controlled stage and Hamamatsu ORCA-Flash4.0 V2 digital CMOS camera. The amplitude and kinetics of the calcium signals were analyzed using custom Matlab code based on work by Laughner and colleagues[56]. When reporting calcium amplitude and dynamics, we first assessed the regularity of the τ_{75} of decay, defined as the standard deviation divided by the mean (SD/mean) of the τ_{75}. Only microtissues with SD/mean of $\tau_{75} < 0.1$ were selected for further analysis.

Supplementary Material

Refer to Web version on PubMed Central for supplementary material.

Acknowledgments

This work was supported by, NIH-NHLBI R01HL096525, R01HL108677, U01HL100406 and U01HL098179, NIH-NIBIB R21EB021003, and in part by NIH-NCATS UH3TR000487. M.Z. acknowledges support from American Heart Association (AHA) postdoctoral fellowship 16POST27750031 and Nappi Family Foundation Research Scholar Project. N.H. acknowledges support from NIH T32 HL007544. M.A.M. acknowledges support

from the Canadian Institute of Health Research Postdoctoral Fellowship 129844. B.S. acknowledges support from California Institute for Regenerative Medicine (CIRM) TBI-01197. We acknowledge assistance from the Berkeley Stem Cell Shared Facility for flow cytometry, the Biological Imaging Facility for confocal microscopy supported by NIH S10 program 1S10RR026866-01, and the Biomolecular Nanotechnology Center for scanning electron microscopy. We thank Elphege Nora and Patrick Devine (Gladstone Institute of Cardiovascular Disease) for helpful discussions and advice regarding p300 expression analysis.

The contents of this publication are solely the responsibility of the authors and do not necessarily represent the official views of CIRM and/or other agencies of the State of California.

B.R.C. is a founder of Tenaya Therapeutics, a company focused on finding treatments for heart failure, including the use of CRISPR interference to interrogate genetic cardiomyopathies. B.R.C. holds equity in Tenaya, and Tenaya provides research support for heart failure-related research to B.R.C. K.E.H. and N.H. have a financial relationship with Organos Inc., and both he and the company may benefit from commercialization of the results of this research.

References

1. Carrier L, Mearini G, Stathopoulou K, Cuello F. Cardiac myosin-binding protein C (MYBPC3) in cardiac pathophysiology. Gene. 573:188–197.2015; [PubMed: 26358504]
2. Strande JL. Haploinsufficiency MYBPC3 mutations: another stress induced cardiomyopathy? Let's take a look! Journal of molecular and cellular cardiology. 79:284–286.2015; [PubMed: 25524041]
3. Feric NT, Radisic M. Maturing human pluripotent stem cell-derived cardiomyocytes in human engineered cardiac tissues. Advanced drug delivery reviews. 96:110–134.2016; [PubMed: 25956564]
4. Mathur A, et al. In vitro cardiac tissue models: Current status and future prospects. Advanced drug delivery reviews. 96:203–213.2016; [PubMed: 26428618]
5. Eng G, et al. Autonomous beating rate adaptation in human stem cell-derived cardiomyocytes. Nature communications. 7:10312.2016;
6. Turnbull IC, et al. Advancing functional engineered cardiac tissues toward a preclinical model of human myocardium. FASEB journal : official publication of the Federation of American Societies for Experimental Biology. 28:644–654.2014; [PubMed: 24174427]
7. Conradi L, et al. Immunobiology of fibrin-based engineered heart tissue. Stem cells translational medicine. 4:625–631.2015; [PubMed: 25947338]
8. Legant WR, et al. Microfabricated tissue gauges to measure and manipulate forces from 3D microtissues. Proceedings of the National Academy of Sciences of the United States of America. 106:10097–10102.2009; [PubMed: 19541627]
9. Mathur A, et al. Human iPSC-based cardiac microphysiological system for drug screening applications. Scientific reports. 5:8883.2015; [PubMed: 25748532]
10. Abramson SV, et al. Pulmonary hypertension predicts mortality and morbidity in patients with dilated cardiomyopathy. Ann Intern Med. 116:888–895.1992; [PubMed: 1580444]
11. Engler AJ, et al. Embryonic cardiomyocytes beat best on a matrix with heart-like elasticity: scar-like rigidity inhibits beating. J Cell Sci. 121:3794–3802.2008; [PubMed: 18957515]
12. Kijlstra JD, et al. Integrated Analysis of Contractile Kinetics, Force Generation, and Electrical Activity in Single Human Stem Cell-Derived Cardiomyocytes. Stem cell reports. 5:1226–1238.2015; [PubMed: 26626178]
13. Liau B, Christoforou N, Leong KW, Bursac N. Pluripotent stem cell-derived cardiac tissue patch with advanced structure and function. Biomaterials. 32:9180–9187.2011; [PubMed: 21906802]
14. Schaaf S, et al. Human engineered heart tissue as a versatile tool in basic research and preclinical toxicology. PloS one. 6:e26397.2011; [PubMed: 22028871]
15. Ribeiro AJ, et al. Contractility of single cardiomyocytes differentiated from pluripotent stem cells depends on physiological shape and substrate stiffness. Proceedings of the National Academy of Sciences of the United States of America. 112:12705–12710.2015; [PubMed: 26417073]
16. Hirt MN, et al. Increased afterload induces pathological cardiac hypertrophy: a new in vitro model. Basic research in cardiology. 107:307.2012; [PubMed: 23099820]
17. Hinson JT, et al. HEART DISEASE. Titin mutations in iPS cells define sarcomere insufficiency as a cause of dilated cardiomyopathy. Science. 349:982–986.2015; [PubMed: 26315439]

18. Stoppel WL, Kaplan DL, Black LD 3rd. Electrical and mechanical stimulation of cardiac cells and tissue constructs. Advanced drug delivery reviews. 96:135–155.2016; [PubMed: 26232525]
19. Kawata S, Sun HB, Tanaka T, Takada K. Finer features for functional microdevices. Nature. 412:697–698.2001; [PubMed: 11507627]
20. Klein F, et al. Elastic fully three-dimensional microstructure scaffolds for cell force measurements. Advanced materials. 22:868–871.2010; [PubMed: 20217807]
21. Jeon H, Hidai H, Hwang DJ, Grigoropoulos CP. Fabrication of arbitrary polymer patterns for cell study by two-photon polymerization process. Journal of biomedical materials research. Part A. 93:56–66.2010; [PubMed: 19484772]
22. Ma Z, et al. Three-dimensional filamentous human diseased cardiac tissue model. Biomaterials. 35:1367–1377.2014; [PubMed: 24268663]
23. Burridge PW, et al. Chemically defined generation of human cardiomyocytes. Nat Methods. 11:855–860.2014; [PubMed: 24930130]
24. Tohyama S, et al. Distinct metabolic flow enables large-scale purification of mouse and human pluripotent stem cell-derived cardiomyocytes. Cell stem cell. 12:127–137.2013; [PubMed: 23168164]
25. Thavandiran N, et al. Design and formulation of functional pluripotent stem cell-derived cardiac microtissues. Proceedings of the National Academy of Sciences of the United States of America. 110:E4698–4707.2013; [PubMed: 24255110]
26. Huebsch N, et al. Miniaturized iPS-Cell-Derived Cardiac Muscles for Physiologically Relevant Drug Response Analyses. Scientific reports. 6:24726.2016; [PubMed: 27095412]
27. Gautel M, Furst DO, Cocco A, Schiaffino S. Isoform transitions of the myosin binding protein C family in developing human and mouse muscles: lack of isoform transcomplementation in cardiac muscle. Circulation research. 82:124–129.1998; [PubMed: 9440711]
28. Bennett PM, Furst DO, Gautel M. The C-protein (myosin binding protein C) family: regulators of contraction and sarcomere formation? Reviews of physiology, biochemistry and pharmacology. 138:203–234.1999;
29. Moss RL, Fitzsimons DP, Ralphe JC. Cardiac MyBP-C regulates the rate and force of contraction in mammalian myocardium. Circulation research. 116:183–192.2015; [PubMed: 25552695]
30. Previs MJ, et al. Molecular mechanics of cardiac myosin-binding protein C in native thick filaments. Science. 337:1215–1218.2012; [PubMed: 22923435]
31. Lan F, et al. Abnormal calcium handling properties underlie familial hypertrophic cardiomyopathy pathology in patient-specific induced pluripotent stem cells. Cell stem cell. 12:101–113.2013; [PubMed: 23290139]
32. Argenziano M, et al. Electrophysiologic Characterization of Calcium Handling in Human Induced Pluripotent Stem Cell-Derived Atrial Cardiomyocytes. Stem cell reports. 10:1867–1878.2018; [PubMed: 29731429]
33. Hidai H, Jeon H, Hwang DJ, Grigoropoulos CP. Self-standing aligned fiber scaffold fabrication by two photon photopolymerization. Biomed Microdevices. 11:643–652.2009; [PubMed: 19130241]
34. Mandegar MA, et al. CRISPR Interference Efficiently Induces Specific and Reversible Gene Silencing in Human iPSCs. Cell stem cell. 2016
35. Musunuru K. Genome editing of human pluripotent stem cells to generate human cellular disease models. Disease models & mechanisms. 6:896–904.2013; [PubMed: 23751357]
36. Harris SP, et al. Hypertrophic cardiomyopathy in cardiac myosin binding protein-C knockout mice. Circulation research. 90:594–601.2002; [PubMed: 11909824]
37. Korte FS, McDonald KS, Harris SP, Moss RL. Loaded shortening, power output, and rate of force redevelopment are increased with knockout of cardiac myosin binding protein-C. Circulation research. 93:752–758.2003; [PubMed: 14500336]
38. de Lange WJ, et al. Neonatal mouse-derived engineered cardiac tissue: a novel model system for studying genetic heart disease. Circulation research. 109:8–19.2011; [PubMed: 21566213]
39. Fraysse B, et al. Increased myofilament Ca2+ sensitivity and diastolic dysfunction as early consequences of Mybpc3 mutation in heterozygous knock-in mice. Journal of molecular and cellular cardiology. 52:1299–1307.2012; [PubMed: 22465693]

40. Chen PP, et al. Dissociation of structural and functional phenotypes in cardiac myosin-binding protein C conditional knockout mice. Circulation. 126:1194–1205.2012; [PubMed: 22829020]
41. Baumgarten G, et al. Myocardial injury modulates the innate immune system and changes myocardial sensitivity. Basic research in cardiology. 101:427–435.2006; [PubMed: 16699746]
42. Birket MJ, et al. Contractile Defect Caused by Mutation in MYBPC3 Revealed under Conditions Optimized for Human PSC-Cardiomyocyte Function. Cell reports. 13:733–745.2015; [PubMed: 26489474]
43. Ribeiro AJS, et al. Multi-Imaging Method to Assay the Contractile Mechanical Output of Micropatterned Human iPSC-Derived Cardiac Myocytes. Circulation research. 120:1572–1583.2017; [PubMed: 28400398]
44. McCain ML, et al. Recapitulating maladaptive, multiscale remodeling of failing myocardium on a chip. Proceedings of the National Academy of Sciences of the United States of America. 110:9770–9775.2013; [PubMed: 23716679]
45. Yang H, et al. Dynamic Myofibrillar Remodeling in Live Cardiomyocytes under Static Stretch. Scientific reports. 6:20674.2016; [PubMed: 26861590]
46. Hirt MN, et al. Deciphering the microRNA signature of pathological cardiac hypertrophy by engineered heart tissue- and sequencing-technology. Journal of molecular and cellular cardiology. 81:1–9.2015; [PubMed: 25633833]
47. Stohr A, et al. Contractile abnormalities and altered drug response in engineered heart tissue from Mybpc3-targeted knock-in mice. Journal of molecular and cellular cardiology. 63:189–198.2013; [PubMed: 23896226]
48. Tanaka A, et al. Endothelin-1 induces myofibrillar disarray and contractile vector variability in hypertrophic cardiomyopathy-induced pluripotent stem cell-derived cardiomyocytes. J Am Heart Assoc. 3:e001263.2014; [PubMed: 25389285]
49. Bostrom P, et al. C/EBPbeta controls exercise-induced cardiac growth and protects against pathological cardiac remodeling. Cell. 143:1072–1083.2010; [PubMed: 21183071]
50. Wei JQ, et al. Quantitative control of adaptive cardiac hypertrophy by acetyltransferase p300. Circulation. 118:934–946.2008; [PubMed: 18697823]
51. He A, Kong SW, Ma Q, Pu WT. Co-occupancy by multiple cardiac transcription factors identifies transcriptional enhancers active in heart. Proceedings of the National Academy of Sciences of the United States of America. 108:5632–5637.2011; [PubMed: 21415370]
52. He A, et al. Dynamic GATA4 enhancers shape the chromatin landscape central to heart development and disease. Nature communications. 5:4907.2014;
53. Dai YS, Cserjesi P, Markham BE, Molkentin JD. The transcription factors GATA4 and dHAND physically interact to synergistically activate cardiac gene expression through a p300-dependent mechanism. J Biol Chem. 277:24390–24398.2002; [PubMed: 11994297]
54. Sunagawa Y, et al. Cyclin-dependent kinase-9 is a component of the p300/GATA4 complex required for phenylephrine-induced hypertrophy in cardiomyocytes. J Biol Chem. 285:9556–9568.2010; [PubMed: 20081228]
55. Hutter JL, Bechhoefer J. Calibration of Atomic-Force Microscope Tips. Rev Sci Instrum. 64:1868–1873.1993;
56. Laughner JI, et al. Processing and analysis of cardiac optical mapping data obtained with potentiometric dyes. Am J Physiol-Heart C. 303:H753–H765.2012;

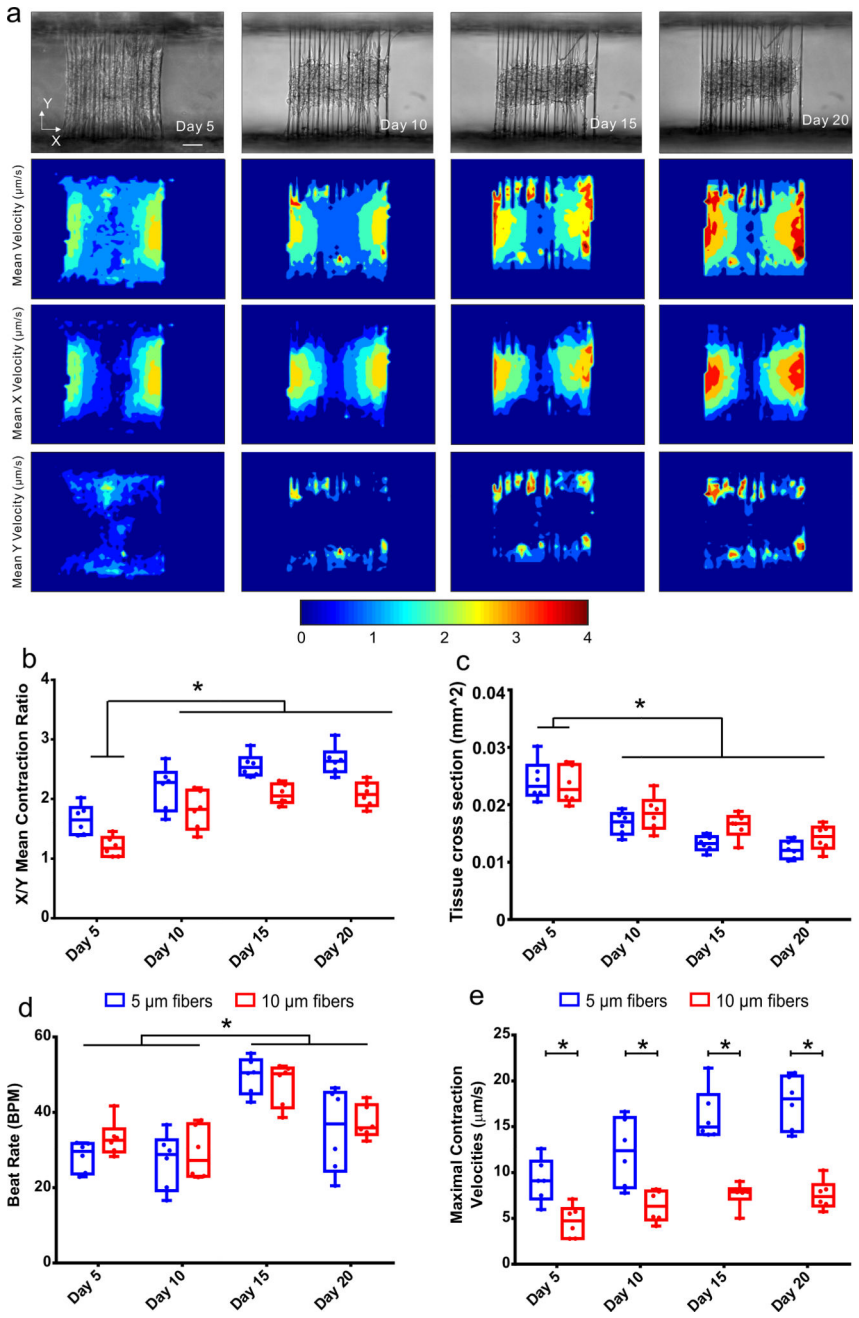

Figure 1. Cardiac microtissues remodeling on filamentous matrices

(a) WT Cardiac microtissues on a 5 μm fiber matrix remodeled their shape from Day 5 to Day 20. Contraction heatmaps showed anisotropic contraction with higher contraction in the X-direction compared to the Y-direction. The motion close to the glass substrates in the heatmaps of mean Y velocity was only resulted from fiber movement during tissue contractions, since no tissue grown at these locations. Scale bar, 100 μm. The progressive tissue remodeling manifested as (b) an increase of the ratio of mean contraction between X-axis and Y-axis directions (ANOVA Bonferroni's multiple comparison test, $p = 0.0086$ for 5 μm matrices and $p = 0.0004$ for 10 μm matrices), and (c) a decrease of the tissue cross-

section (Z-Y direction) by comparing Day 5 to Day 10–20 (ANOVA Bonferroni's multiple comparison test, $p = 0.0001$ for 5 μm matrices and $p = 0.0135$ for 10 μm matrices). (d) The beat rate of cardiac microtissues slightly increased comparing Day 5–10 and Day 15–20 (two-tailed student t-test, $p = 0.005$ for 5 μm matrices and $p = 0.004$ for 10 μm matrices). By investigating the effect of tissue mechanical environment on cardiac contractility, we found (d) no significant difference on beat rate, but (e) much higher maximal contraction velocity for the cardiac microtissues assembled on 5 μm matrices than the ones on 10 μm matrices (two-tailed student t-test, $p = 0.0035$ for Day 5, $p = 0.0052$ for Day 10, $p = 0.000131$ for Day 15, and $p = 0.0000415$ for Day 20). Data ($n = 6$): box plot with minimum, maximum, median, 25% and 75%.

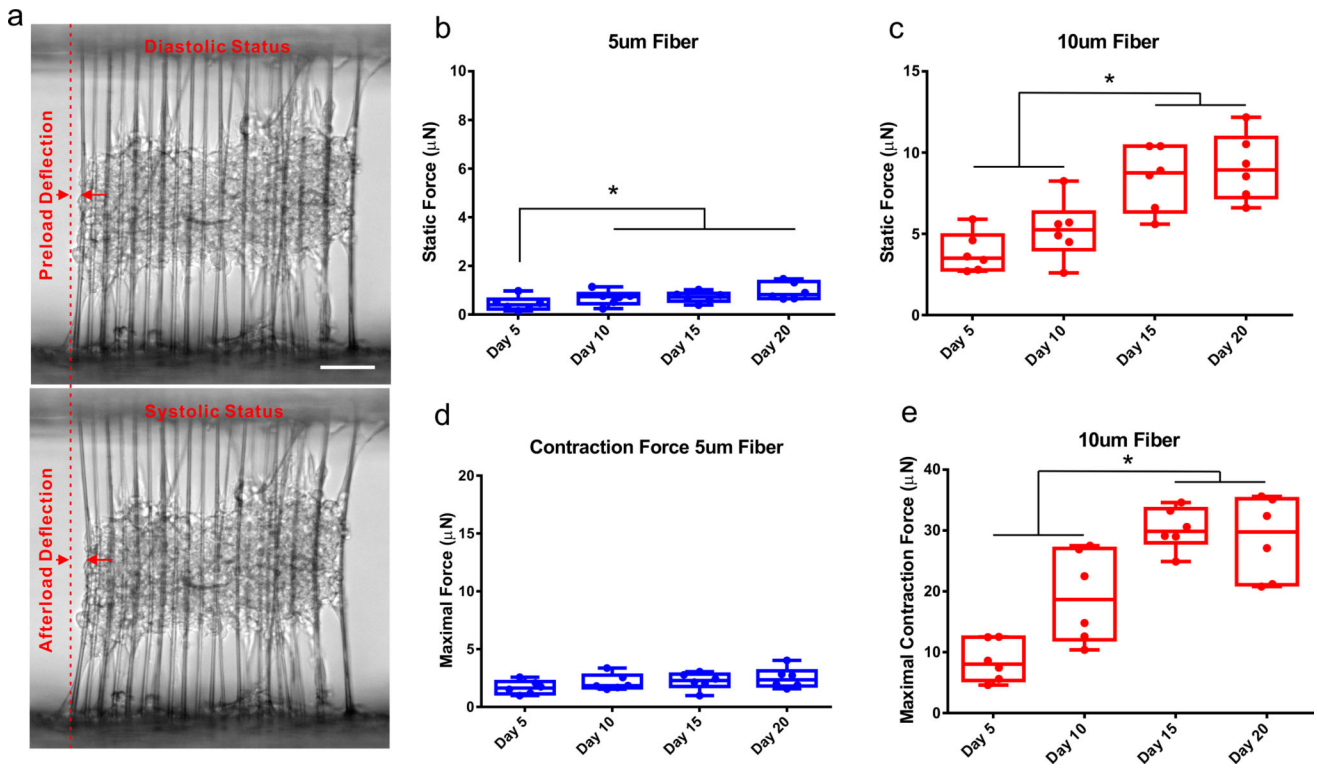

Figure 2. Force measurement based on fiber deflection

(a) The static force and contraction force were calculated based on preload deflection at diastolic status and afterload deflection at systolic status. Scale bar, 100 μm. The static forces increased during 20-days culturing for WT cardiac microtissues assembled on both (b) 5 μm and (c) 10 μm matrices (ANOVA Bonferroni's multiple comparison test, p = 0.0499 for 5 μm matrices and p = 0.0387 for 10 μm matrices). (d) The contraction forces showed no significant increase for WT cardiac microtissues on 5 μm matrices, (e) whereas the increase became significant for the microtissues on 10 μm matrices (ANOVA Bonferroni's multiple comparison test, p = 0.0147 for 10 μm matrices). At each time point, the magnitudes of the static and contraction forces were significantly higher for WT cardiac microtissues grown on 10 μm matrices than the ones grown on 5 μm matrices. Data (n = 6): box plot with minimum, maximum, median, 25% and 75%.

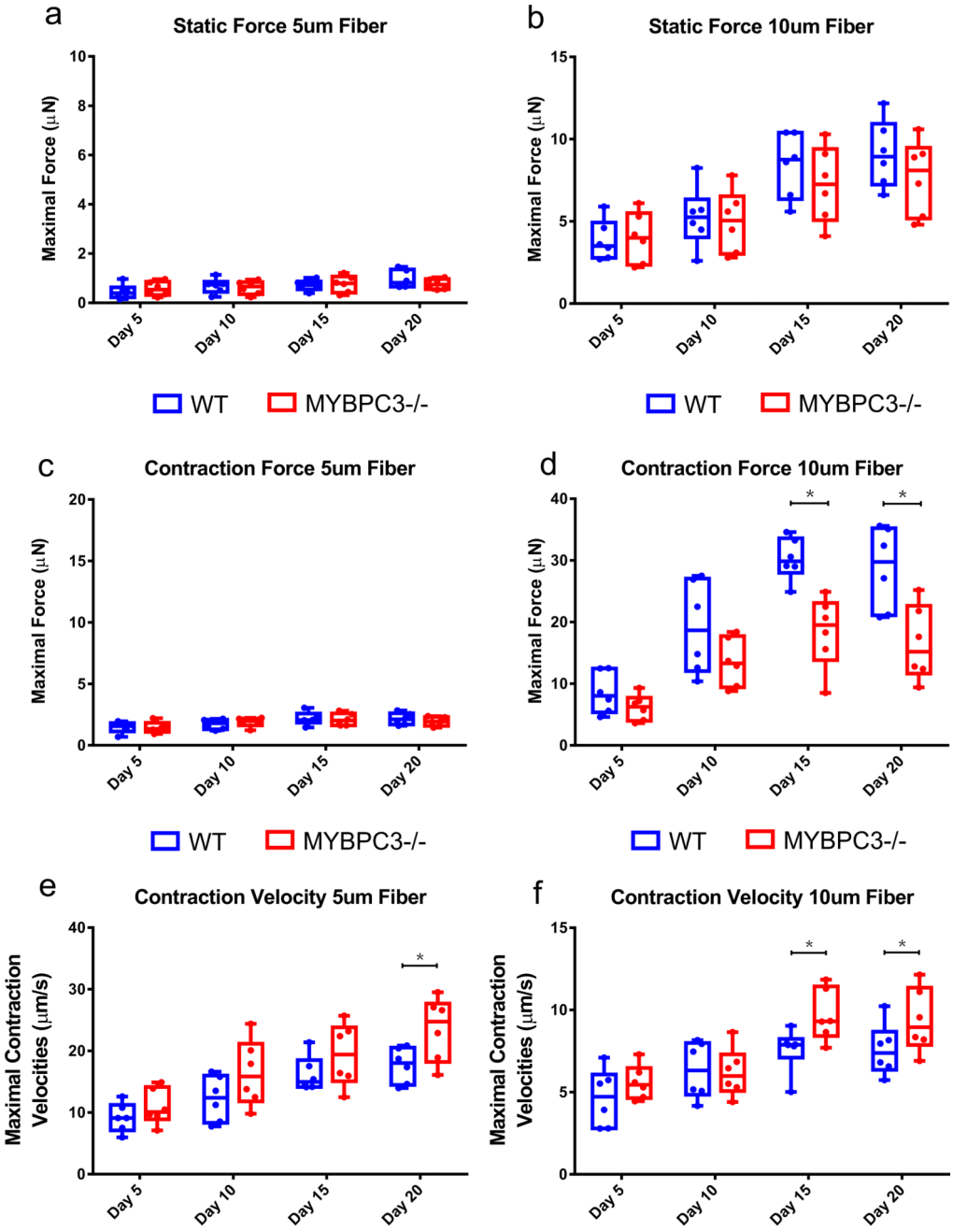

Figure 3. Contractile deficits of MYBPC3$^{-/-}$ cardiac microtissues

Comparing WT to MYBPC3$^{-/-}$ cardiac microtissues showed no significant difference on static forces for the microtissues on both (a) 5 μm and (b) 10 μm matrices, and (c) no difference on contraction forces for the microtissues on 5 μm matrices, (d) but lower contraction forces at Day 15 & 20 for the MYBPC3$^{-/-}$ microtissues only on 10 μm matrices (two-tailed student t-test, $p = 0.0016$ for Day 15, $p = 0.0081$ for Day 20). MYBPC3$^{-/-}$ cardiac microtissues showed higher maximal contraction velocity for the cardiac microtissues assembled on both (e) 5 μm (two-tailed student t-test, $p = 0.0366$ for Day 20) and (f) 10 μm matrices (two-tailed student t-test, $p = 0.0388$ for Day 15, $p = 0.0475$ for Day

20) compared to WT cardiac microtissues. At each time point, the magnitudes of the static and contraction forces were significantly higher for WT and MYBPC3$^{-/-}$ cardiac microtissues grown on 10 μm matrices, and contraction velocities were significantly higher for the microtissues grown on 5 μm matrices. Data (n = 6): box plot with minimum, maximum, median, 25% and 75%.

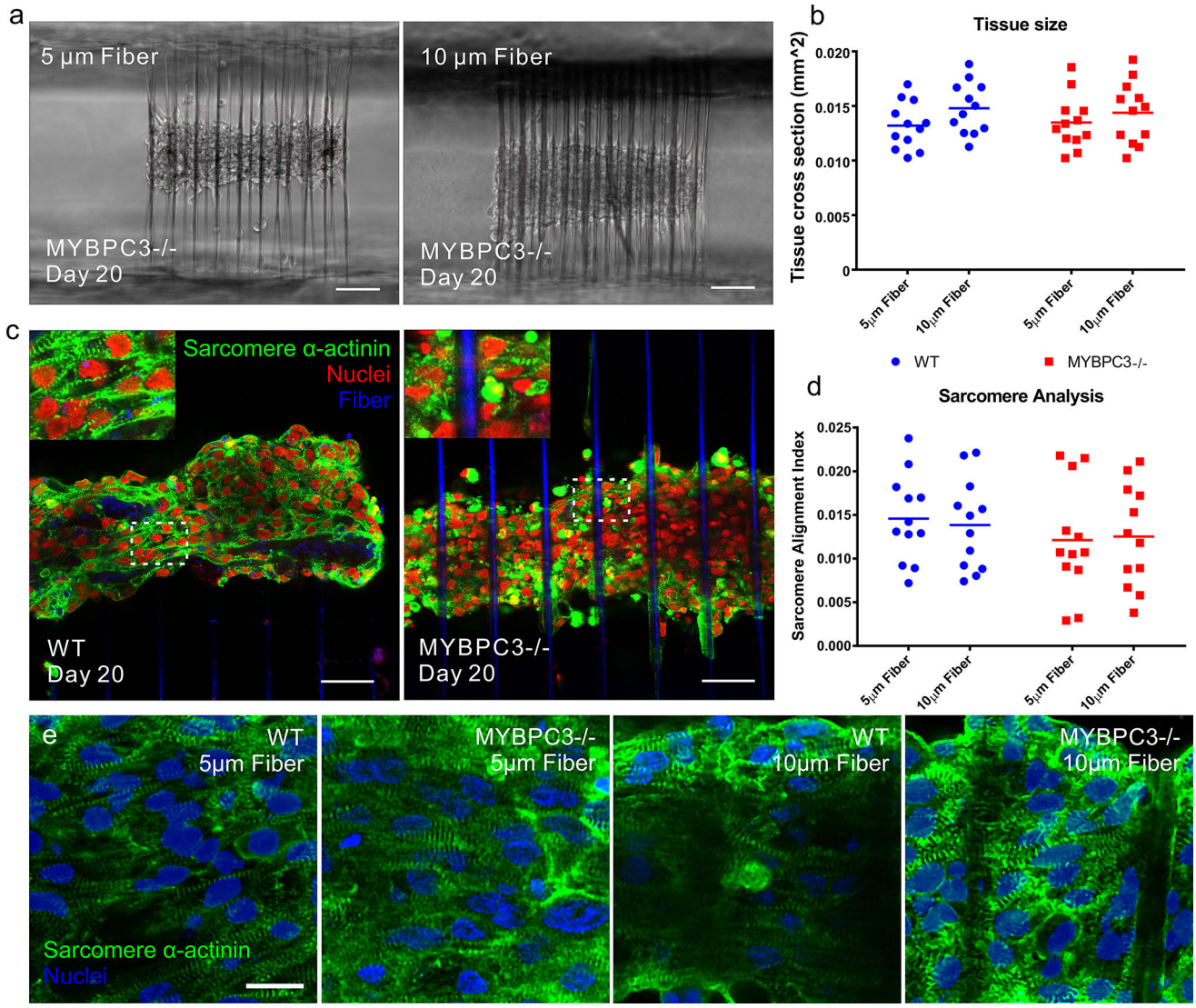

Figure 4. No structural disarray on MYBPC3$^{-/-}$ cardiac microtissues

(a) Bright-field microscopy showed (b) no significant difference on tissue cross-section between WT and MYBPC3$^{-/-}$ cardiac microtissues assembled on 5 μm and 10 μm matrices at Day 20. Scale bar, 100 μm. (c) Confocal microscopy showed (d) no significant difference on sarcomere alignment index between WT and MYBPC3$^{-/-}$ microtissues assembled on 5 μm and 10 μm matrices at Day 20. Scale bar, 50 μm. Confocal images of (e) sarcomere organization of WT and MYBPC3$^{-/-}$ cardiac microtissues growing on 5 μm and 10 μm fiber matrices. Scale bar, 20 μm. Data b&d (n = 12): mean with all data points. Image e&f: representative confocal images of 12 samples.

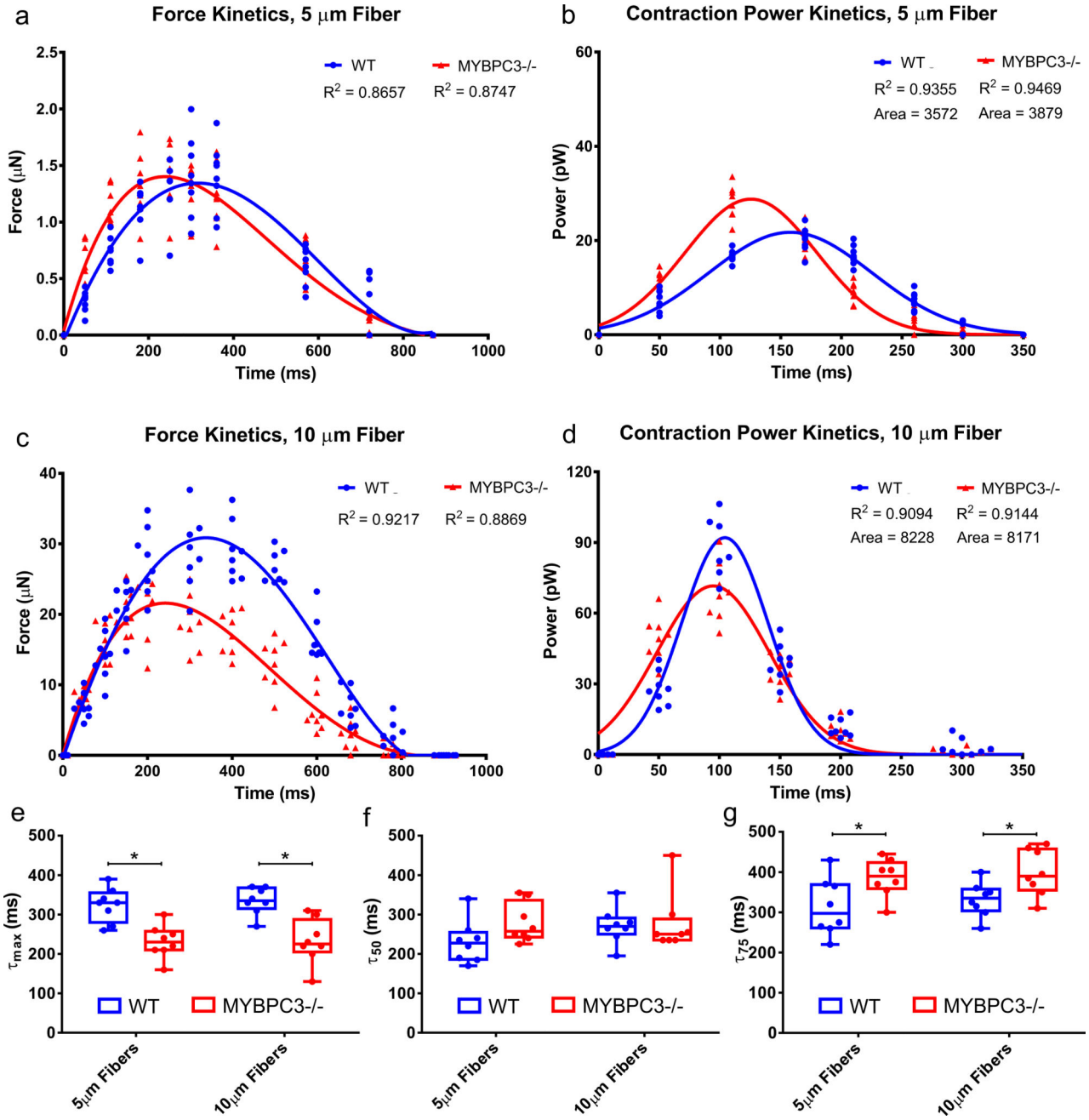

Figure 5. Mechanical load altered contractile force dynamics

(a) The force development of MYBPC3$^{-/-}$ cardiac microtissues on 5 μm matrices was faster than WT tissues, but no difference in the magnitude. (b) MYBPC3$^{-/-}$ cardiac microtissues on 5 μm matrices showed higher power output and energy consumption compared to WT microtissues. (c) MYBPC3$^{-/-}$ cardiac microtissues on 10 μm matrices showed (c) impaired force generation and (d) lower power output compared to WT microtissues. (e) MYBPC3$^{-/-}$ cardiac microtissues had faster contraction reaching to the peak force (τ_{max}) compare to the WT microtissues (two-tailed student t-test, $p = 0.000633$ for 5 μm matrices, $p = 0.000104$ for 10 μm matrices). (f) Although no significant difference on early decay time of 50% peak

force (τ_{50}), (g) MYBPC3$^{-/-}$ cardiac microtissues had a longer late decay time of 75% peak force (τ_{75}) (two-tailed student t-test, $p = 0.00315$ for 5 μm matrices, $p = 0.0194$ for 10 μm matrices). Data a–d ($n = 8$): all data with curve fitting. Data e–g ($n = 8$): box plot with minimum, maximum, median, 25% and 75%.

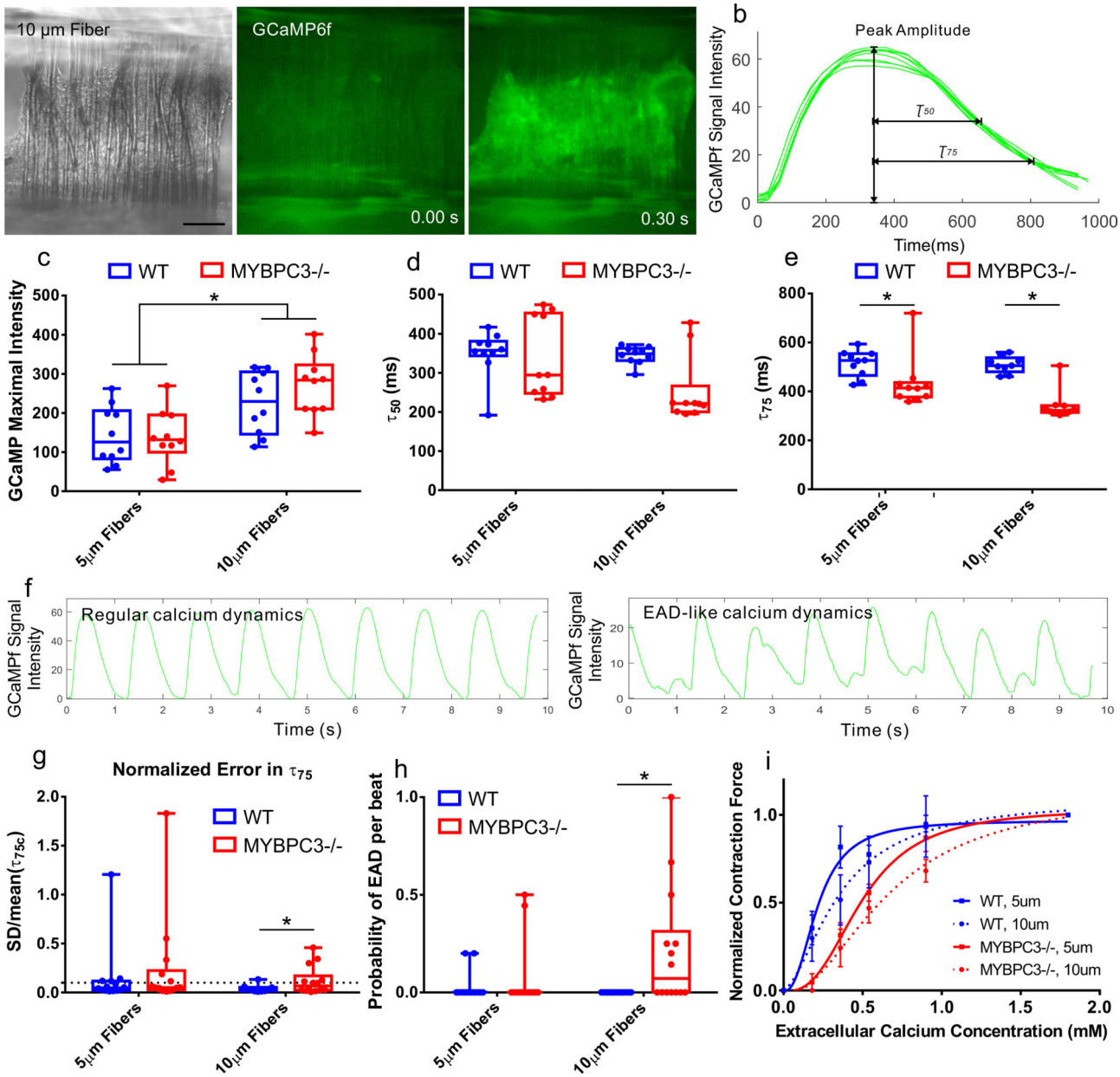

Figure 6. Calcium transient abnormalities on MYBPC3$^{-/-}$ cardiac microtissues

(a) The calcium fluctuation of a GCaMP6f-WT cardiac microtissue growing on a 10 μm fiber matrix. (b) We were able to quantify the calcium dynamics based on the GCaMP fluorescent intensity recorded from GCaMP6f cardiac microtissues. (c) Cardiac microtissues growing on 10 μm matrices had higher peak intensity comparing to the ones on 5 μm matrices (two-tailed student t-test, $p = 0.0288$ for WT, $p = 0.00152$ for MYBPC3$^{-/-}$). (d) Although there was no significant difference on early decay time (τ_{50}), (e) GCaMP6f-MYBPC3$^{-/-}$ cardiac microtissues had a shortened late decay time (τ_{75}) on both 5 μm and 10 μm fiber matrices (two-tailed student t-test, $p = 0.00104$ for 5 μm matrices, $p = 0.000162$ for 10 μm matrices). (f) Representative traces for regular calcium dynamics and EAD-like calcium dynamics measured from GCaMP6f-MYBPC3$^{-/-}$ cardiac microtissues. The

GCaMP6f-MYBPC3$^{-/-}$ cardiac microtissues showed significant (g) higher variations on normalized error in τ_{75} (two-tailed student t-test, $p = 0.0253$ for 10 μm matrices) and (h) higher possibility of EAD behaviors when growing on 10 μm matrices (two-tailed student t-test, $p = 0.0178$ for 10 μm matrices). (i) Calcium desensitization was found on MYBPC3$^{-/-}$ cardiac microtissues comparing to WT microtissues, and microtissues contracting against stiffer fibers. Data c–h ($n = 10$): box plot with minimum, maximum, median, 25% and 75%. Data i ($n = 6$): mean ± SD.

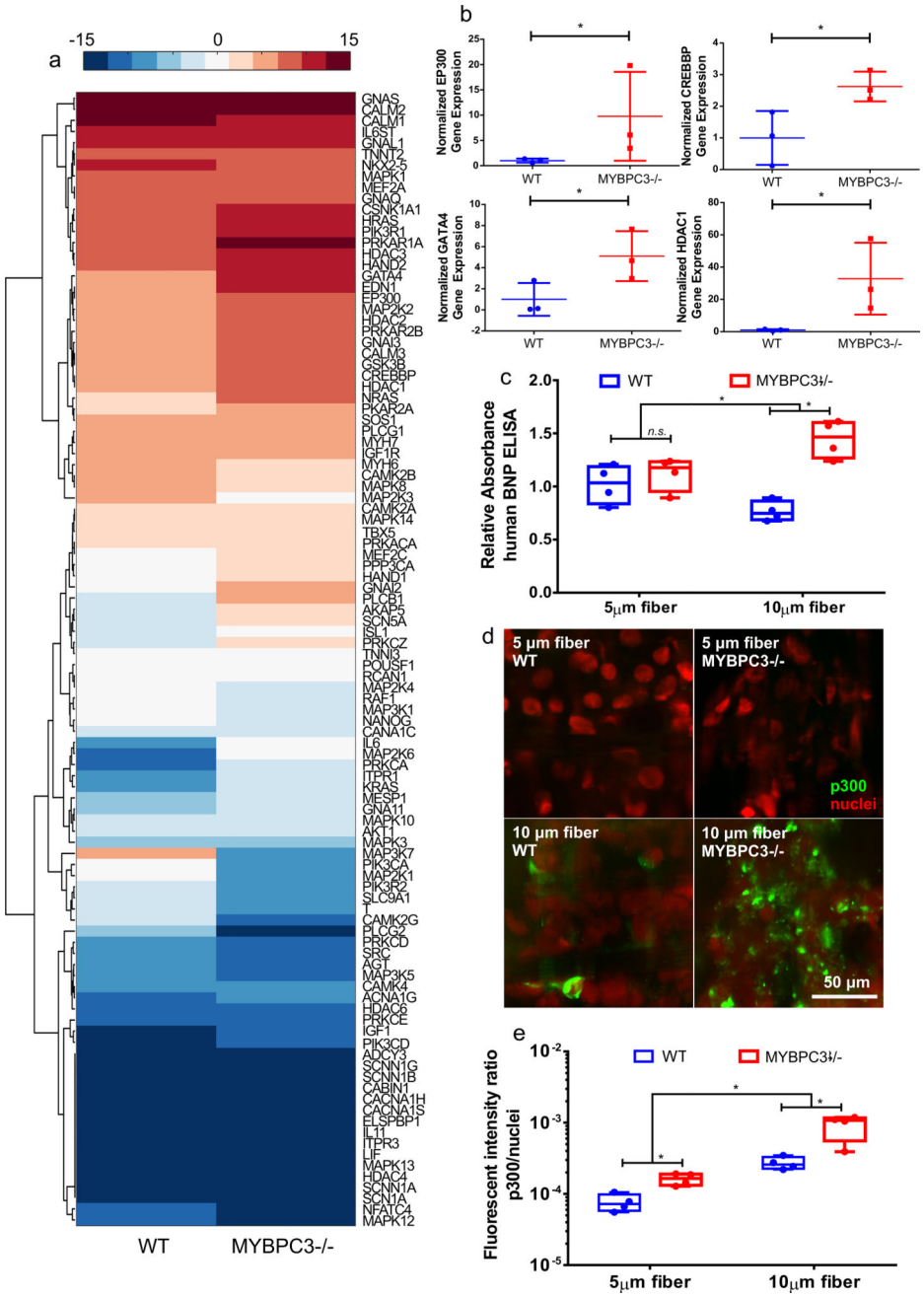

Figure 7. EP300-GATA4 directed contractile deficits due to mechanical stress

(a) At Day 20, 102 genes were profiled for WT and MYBPC3$^{-/-}$ cardiac microtissues growing on 10 μm matrices. (b) Gene expression of EP300 (p = 0.0798), CREBBP (p = 0.022), HDAC1 (p = 0.0331) and GATA4 (p = 0.034) on MYBPC3$^{-/-}$ cardiac microtissues significantly increased compared to WT cardiac microtissues grown on 10 μm filamentous matrices (two-tailed student t-test). (c) At Day 20, human BNP expression on MYBPC3$^{-/-}$ cardiac microtissues was found to be significantly higher than WT cardiac microtissues only grown on 10 μm matrices (two-tailed student t-test, p = 0.0478 for matrices comparison, p = 0.0015 for WT/ MYBPC3$^{-/-}$ comparison on 10 μm matrices). (d) Confocal images of p300

fluorescent staining on both WT and MYBPC3$^{-/-}$ cardiac microtissues on 5 μm and 10 μm filamentous matrices. (e) Quantitative fluorescent analysis on p300 expression showed the cardiac microtissues on 10 μm matrices had higher p300 expression than the ones on 5 μm matrices, and MYBPC3$^{-/-}$ cardiac microtissues had higher p300 expression than WT microtissues (two-tailed student t-test, $p = 0.0269$ for matrices comparison, $p = 0.00504$ for WT/ MYBPC3$^{-/-}$ comparison on 5 μm matrices, $p = 0.0345$ for WT/ MYBPC3$^{-/-}$ comparison on 10 μm matrices). Data b ($n = 3$): mean ± SD with all data. Data c ($n = 4$): box plot with minimum, maximum, median, 25% and 75%. Data e ($n = 6$): box plot with minimum, maximum, median, 25% and 75%.